

We are IntechOpen, the world's leading publisher of Open Access books Built by scientists, for scientists

5,000

Open access books available

125,000

International authors and editors

140M

Downloads

Our authors are among the

154

Countries delivered to

TOP 1%

most cited scientists

12.2%

Contributors from top 500 universities



WEB OF SCIENCE™

Selection of our books indexed in the Book Citation Index
in Web of Science™ Core Collection (BKCI)

Interested in publishing with us?
Contact book.department@intechopen.com

Numbers displayed above are based on latest data collected.
For more information visit www.intechopen.com



Modeling and Simulation of Switched Reluctance Machines

Mahmoud Hamouda and László Számel

Abstract

This chapter discusses the modeling and simulation approaches for switched reluctance machines (SRMs). First, it presents the modeling methods for SRMs including analytical models, Artificial intelligence based models, and lookup tables based models. Furthermore, it introduces the finite element method (FEM) and experimental measurement methods to obtain high fidelity magnetic characteristics for SRMs. Step-by-step procedure is explained for SRM modeling and analysis using FEM. The direct and indirect measurement methods of SRM magnetic characteristics are included, comparison between the measured and FEM-calculated characteristics is achieved, and good agreement is seen. In addition, this chapter gives the mathematical modeling of SRM, and explains its model development using MATLAB/Simulink environment. Simulation and experimental results are obtained, a very good agreement is observed.

Keywords: switched reluctance machines, magnetic characteristics, analytical models, artificial intelligent models, lookup tables, finite element analysis, experimental measurement, MATLAB simulation

1. Introduction

Accurate modeling of switched reluctance machines (SRMs) is the key stone for developing and optimizing different control strategies. Accurate prediction of machine performance under transient and steady-state conditions requires precise knowledge of its magnetic characteristics. However, the doubly salient structure, deep magnetic saturation, switching form of supply, and highly nonlinearity make it very complicated to accurately model the magnetic characteristics of SRMs [1–4]. Several approaches are used to model the magnetic characteristics of SRMs including analytical models, artificial intelligent models, and lookup tables based models [5, 6].

The analytical models can be derived directly from machine geometry, and magnetic theory [4, 7–10]. They can also be driven from the previously obtained data using finite element analysis (FEA) or experimental measurements [11–15].

Intelligent techniques such as fuzzy logic and artificial neural networks (ANNs) are inherently suitable to model the nonlinear characteristics of SRMs. They have been reported for SRM modeling in [16–19]. However, the training needs high skills and a large number of given data. It should be noted that although the accuracies of aforementioned intelligence methods are relatively high, they still demand substantial measured samples to train the network or generate the rules.

For the lookup tables' techniques, the models are commonly based on interpolation and extrapolation. The accuracy of the lookup table methods heavily depends on the number of stored samples. The data can be obtained by FEA or measurements with efficient resolution to achieve a highly trusted model [20, 21].

The analytical functions and the intelligent approaches introduce errors in the model and even the ones capable of a high grade approximation are usable only on certain machines. The output quantities have values different from the real ones measured on the test bench, making the model unusable for the optimization of the geometry and/or control. Thus the need of building models based directly on the magnetization curves obtained by FEA or by measurements on a test bench, capable of taking into account all nonlinearities and eliminating all inaccuracies arose. In the early days, the process of modeling electromagnetic field of SRMs with FEM based software was considered slow and demanding, but nowadays with the evolution of computers the FEM analysis has become imperative in describing the behavior of SRMs. Therefore, this chapter focuses on the modeling of SRM using data obtained from FEA or measurements in form of lookup tables.

2. Analytical modeling of SRM

Analytical models play an important role to easy the machine analysis as the integrations and differentiations are easier to be performed analytically. They can be of great help in the initial estimations of machine torque, efficiency that is required for the better selection of machine drive, where a trade-off between model accuracy and computation time can be made [5]. For high performance SRM drive, sometimes accurate analytical models become indispensable for machine simulation and real-time implementation as it is may be the simplest.

Several researches have been directed to analytically model SRM directly from its physical information. In order to express the idea of analytical models, an example is explained as follows. In [7], an analytical model is derived based on a piecewise analysis of machine fundamental geometry and turns per phase. The flux is represented by Eq. (1) as follows:

$$\lambda(i, \theta) = a_1(\theta) \left[1 - e^{[a_2(\theta)i]} \right] + a_3(\theta)i \quad (1)$$

where i is the motor current, θ is the rotor position, and $a_1(\theta)$, $a_2(\theta)$, and $a_3(\theta)$ are the unknown coefficient that needs to be calculated. The incremental inductance can be obtained from flux derivative as:

$$l(i, \theta) = \frac{\partial \lambda(i, \theta)}{\partial i} = -a_1(\theta) \cdot a_2(\theta) \cdot e^{[a_2(\theta)i]} + a_3(\theta) \quad (2)$$

Unsaturated phase inductance (L) can be represented as a function of rotor angle as:

$$L(\theta) = -a_1(\theta) \cdot a_2(\theta) + a_3(\theta) \quad (3)$$

Equation (3) is rearranged as,

$$a_2(\theta) = \frac{a_3(\theta) - L(\theta)}{a_1(\theta)} \quad (4)$$

The unknown coefficients $a_1(\theta)$, $a_3(\theta)$, and $L(\theta)$ are functions of rotor angle and needed to be determined. **Figure 1** shows the proposed piecewise linear models for these coefficients. The angle θ_a and θ_u refer to the aligned and unaligned rotor positions respectively. From θ_a to θ_1 , the stator and rotor pole arcs are fully covered. After θ_1 , the rotor pole arc starts to uncover stator pole arc. At θ_2 , the pole arcs become fully uncovered. Eleven parameters are included to be determined in calculation process that are four Magnetization coefficients ($a_1(\theta_a)$, $a_3(\theta_a)$, $a_1(\theta_u)$, $a_3(\theta_u)$), three Inductive constant (L_{max} , L_{min} , L_{corner}), and four angular breakpoints (θ_1 , θ_1' , θ_2 , θ_u). The angular breakpoints are found directly from motor design parameter. Inductive constant L_{max} is found from Eq. (3), while determination of L_{corner} and L_{min} require dimensional detail of the rotor and stator poles. The magnetization coefficient $a_1(\theta_a)$ and $a_3(\theta_a)$ are found iteratively. Step-by-step procedure of finding each parameter is covered in [7].

In [8], an analytical model for SRM is derived using the flux tube method. It divides the angle between the aligned and the unaligned positions into three regions. In [9, 10], the analytical model is derived from the equivalent magnetic circuits of SRM. In [4], a proposed method of determining the stator winding flux linkages and torque of a fully pitched mutual coupled SRM is presented.

A popular method for analytical model development of SRMs is to fit the previously obtained magnetic characteristics using analytical formulations. In [22], an exponential equation is used for SRM modeling. It was not enough to achieve an adequate model. Hence, an additional term depending on rotor position was introduced in [23]. In [5, 24], exponential functions are used for SRM modeling. It has a better accuracy, but requires intensive computation to find model parameters using least square method. In [25–27], Fourier series is used for SRM modeling. But the determination of Fourier series coefficients is complicated.

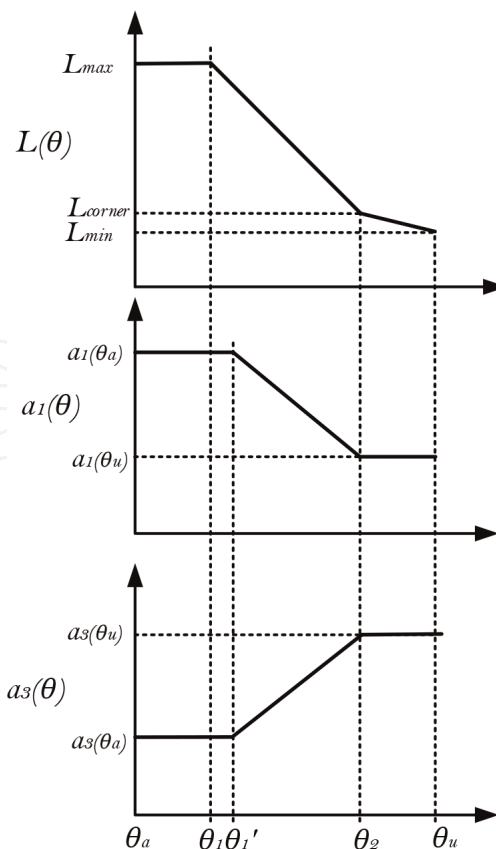


Figure 1. Piecewise linear model assumed for unsaturated phase inductance, magnetization coefficient a_1 and a_3 , as a function of rotor angle θ .

3. Artificial intelligence-based models

Among the artificial intelligence techniques, fuzzy logic and artificial neural networks (ANNs) are employed to model the nonlinear magnetic characteristics of SRMs. They have been reported in SRM modeling in [28–31]. In [28], a two-layer recurrent ANN is employed to identify the damper currents and resistance of phase winding from operating data. By this modeling method, the accurate nonlinear model can be obtained. Likewise, complex expressions and fitting algorithms are circumvented. In [29], a four-layer back-propagation (BP) ANN is applied to estimate the electromagnetic characteristics under the stator winding fault condition. Similarly, fuzzy logic systems also have strong nonlinear approximation ability. In [30], a fuzzy logic system is adopted to describe the electromagnetic characteristics, which shows high reliability and robustness. On this basis, an improved fuzzy logic system is implemented in [31] and it only requires 264 rules compared to nearly 1000 rules in [30] while maintaining a high accuracy. It should be noted that the intelligence methods requires a high number of measured samples to train the network or generate the rules.

4. Finite element analysis of SRM

It is well known that finite element method (FEM) is used to determine the magnetic vector potential over complex geometry with nonlinear magnetic characteristics such as SRMs. In the early days, the process of modeling electromagnetic field of SRMs with FEM based software was considered slow and demanding, but the recent programs for finite element analysis (FEA) make the calculation of SRM magnetization characteristics much easier and speed up computations by static magnetic field analysis. Lately, several software programs are available for FEA that can provide 2D or 3D analysis. The 3D software may require longer time but provides better accuracy. The 2D software can provide the required accuracy with proper settings, which can efficiently save time and effort. Hence, 2D FEA for SRMs is a good choice; it can provide accuracy similar to 3D FEA [13]. FEMM (Finite Element Method Magnetics) is a free 2D software for FEA, it has a basic advantages of being executed using MATLAB. Only an Octave is needed to link FEMM with MATLAB. It needs only 1/4 of the stator geometry to draw/represent the complete motor. The complete analysis and output data storage can be executed and plotted using MATLAB, which can provide an easy way for machine analysis and optimization. Therefore, FEMM is used in this work.

4.1 Equations used for FEA

A set of equations describing the problem is given below. The magnetic flux density B in a magnetic material can be given as [32],

$$B = \mu H = \frac{H}{\gamma} \quad (5)$$

where H is the magnetic field density, μ is permeability of the magnetic material and γ is the reluctivity of the magnetic material. From Ampere's law,

$$\text{curl}(B) = \mu J_o \quad (6)$$

where J_o is the current density.

Defining the magnetic vector potential A as,

$$B = \text{curl}(A) \quad (7)$$

$$\text{curl}(\text{curl}(A)) = \mu J_o \quad (8)$$

Setting $\nabla \cdot A = 0$, and from the vector identity for the curl of the curl of the vector,

$$\nabla(\nabla \cdot A) - \nabla^2 A = \mu J_o \quad (9)$$

This implies that,

$$\nabla^2 A = -\mu J_o \quad (10)$$

Using the assumption (c) below, the above expression can be written as,

$$\frac{\partial}{\partial x} \frac{\partial A}{\partial x} + \frac{\partial}{\partial y} \frac{\partial A}{\partial y} = -\mu J_o \quad (11)$$

The solution of Eq. (11) gives the magnetic vector potential A inside the motor. It is obtained using an interpolation technique to minimize the nonlinear energy functional,

$$F = \int_Q \left[\int_0^B H \cdot dB - \int_0^A J_o \cdot dA \right] dQ \quad (12)$$

where Q is the problem region of integration.

The entire problem region Q is subdivided into triangular finite elements. The elements are defined such that the sides of the triangles coincide with the boundary of each material. FEMM implements this by allowing the placement of nodes on each of the boundaries. The following assumptions are made to estimate the magnetic field inside SRM [14, 21, 32]:

The outer surface of the stator is treated as line of a zero magnetic vector potential. The nodes along this flux are defined using Dirichlet boundary condition.

- a. The magnetic materials of the stator and rotor are isotropic
- b. The magnetic vector potential and current density have z-directed components only.
- c. The stator windings are identical and positioned symmetrically along the stator bore.
- d. The stator and rotor are concentric and the air gap which separates them has constant width at aligned position.
- e. The end effects, hysteresis effects, the skin effect are neglected.

4.2 Modeling of SRM using FEA

Modeling of SRM using FEMM requires three sequential stages. The first stage is to read the motor dimensions and plot its geometry. The second stage defines the

materials properties over machine geometry, circuits, and boundary conditions. The final stage analyses the machine and calculates the desired magnetic characteristics. The code is written using FEM-Octave to link FEMM software with MATLAB software. The FEM-Octave file contains all the required functions to draw, define and analysis the studied geometry [33].

Before starting of geometry plotting, it is needed to open a new FEMM file with the desired settings. For SRM analysis, the new file is an electromagnetic problem with the following definitions:

```
%% Open a new magnetics problem
La =15.1; % The SRM stack length
addpath('C:\femm42\mfiles');
savepath;
openfemm;
newdocument(0); % 0 means magnetics problem
mi_probdef(0,'centimeters','planar',1.e-8,la,30); % problem definitions
```

4.2.1 Geometry plotting

The FEM-based electromagnetic analysis of an SRM starts by creating the geometry of real machine. The geometrical dimensions of the studied 8/6 SRM are gathered in **Table 1**. **Figure 2** shows the cross-sectional area of SRM considering the symmetry along the length of the machine.

After the geometrical parameters are known, a lot of mathematical formulation should be deduced to define the Cartesian coordinates for each corner point in this geometry (in our case the SRM). The studied machine is an 8/6 SRM, it has 8 stator poles and 6 rotor poles as shown in **Figure 2**. The SRM has a symmetrical geometry. Only one rotor pole can be drawn and rotated five more times with 60° shift, the

Geometry parameter	Symbol	Value
Output power (kW)	—	4
Rated voltage (V)	—	600
Rated RMS current (A)	—	9
Rated speed (r/min)	—	1500
Turns per pole	N	88
Phase resistance (Ω)	R	0.64 Ω
Shaft diameters	D_{sh}	36
Bore diameters	D_{bore}	96.7
Stator outside diameter	D_{oy}	179.5
Height of rotor pole	h_{tr}	18.1
Height of stator pole	h_{ts}	29.3
Air-gap length	l_g	0.4
Rotor pole arc	β_r	21.5°
Stator pole arc	β_s	20.45°
Stack length	L_{st}	151

Table 1.
The design data of SRMs in mm.

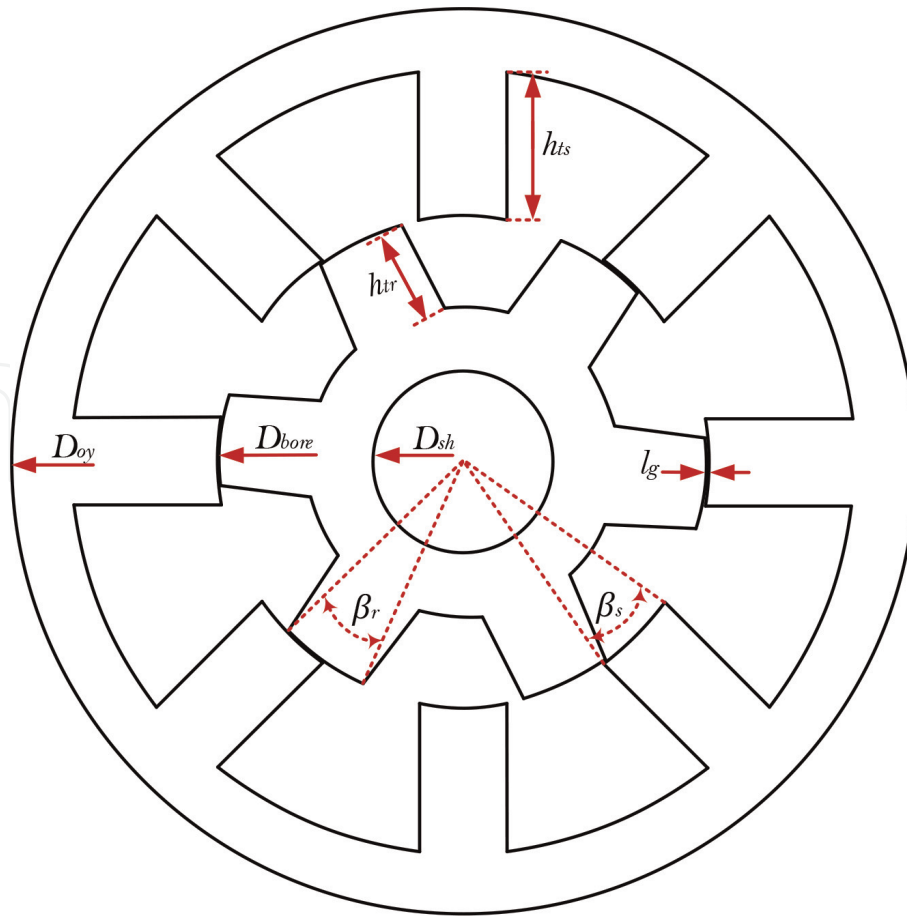


Figure 2.
 The cross-sectional area of 8/6 SRM.

same can be done for the stator but the rotation will be seven more times with 45° shift. The procedure is well explained through the following **Figures 3–5**.

After the calculation of the required (x, y) coordinates for one rotor pole, it can be plotted as shown in **Figure 3(a)**. One rotor pole is drawn by the definition of 5 points (P1-p5). First, the five points need to be added to the FEMM file, after that the connection between points is achieved. Using the Octave functions (mi_addnode, mi_addsegment, and mi_addarc) to connect between the points as follows:

```
%% rotor points
mi_addnode(x_p1,y_p1);
mi_addnode(x_p2,y_p2);
mi_addnode(x_p3,y_p3);
mi_addnode(x_p4,y_p4);
mi_addnode(x_p5,y_p5);

%% connect between rotor points
mi_addsegment(x_p1,y_p1,x_p2,y_p2); % segment P1 - p2
mi_addsegment(x_p3,y_p3,x_p4,y_p4); % segment P3 - p4
mi_addarc(x_p3,y_p3,x_p2,y_p2,theta32,5); % arc-segment P3 - p2
mi_addarc(x_p5,y_p5,x_p4,y_p4,theta54,5); % arc-segment P5 - p4
```

The variable (theta32) is the angle of arc-segment that connects points P3 and p2. Noting that the arc is drawn counterclockwise direction with 5 segments. After drawing of one rotor pole, the other poles can be drawn by copying and rotation of this pole with 60° shift. The rotation function is (mi_copyrotate). It needs first to select the parts that will be rotated. For the rotor pole, the rotated parts are 2

segments (segment P1-p2, segment P4-p3,) and 2 arc-segments (arc-segment P2-p3, arc-segment P4-p5). The following MATLAB script explains the process:

```

%% Select the rotor parts that will be rotated
mi_clearselected; % clears all the selected parts
mi_selectsegment(x_p1,y_p1); % select segment P1 - p2
mi_selectsegment(x_p4,y_p4); % select segment P4 - p3
mi_selectarcsegment(x_p2,y_p2); % select arc-segment P2 - p3
mi_selectarcsegment(x_p4,y_p4); % select arc-segment P4 - p5
mi_copyrotate(0, 0, 60, 6) ; % rotate selected parts around (0,0)
mi_clearselected;
    
```

After the rotation, the rotor will be completely drawn as shown in **Figure 3(b)**. The same procedure can be done for the stator pole including the windings. One stator pole can be drawn by the definition of (x, y) coordinates of 13 points (P6-p18) as shown in **Figure 4(a)**. The final stator poles will be as shown in **Figure 4(b)**. The complete geometry of SRM is shown in **Figure 5**.

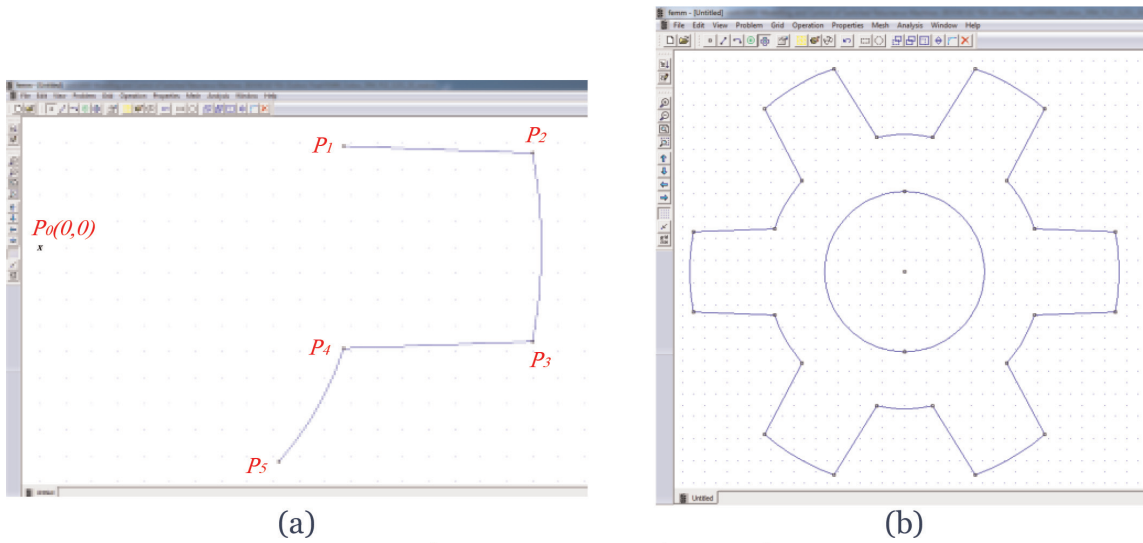


Figure 3. The rotor plotting for 8/6 SRM. (a) One rotor pole drawing (b) The complete rotor drawing.

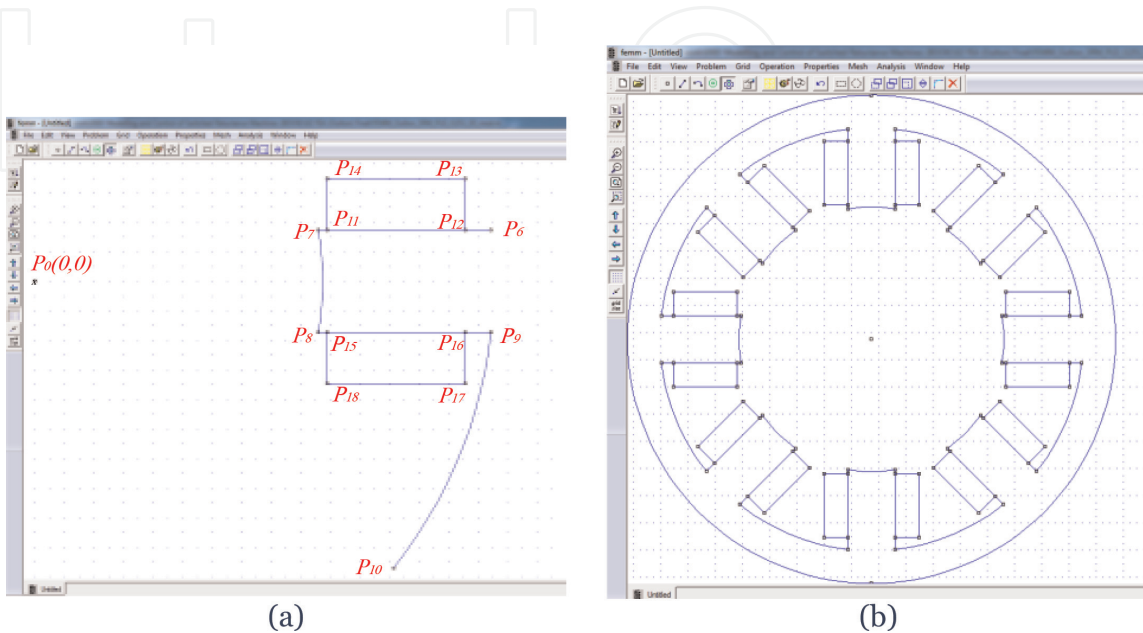


Figure 4. The stator plotting for 8/6 SRM. (a) One stator pole drawing (b) The complete stator drawing.

4.2.2 Definition of materials, circuits and boundary conditions

4.2.2.1 Definition of materials properties

After defining the geometry, it is necessary to attribute to each area its magnetic properties of the corresponding material. The areas of air and copper winding are set with a unitary relative magnetic permeability. It is important to note that the central circular area as shown in **Figure 3(b)** is not filled by air but corresponds to machine shaft that is made of a nonmagnetic material with a unitary relative magnetic permeability. Hence, the shaft can be considered as air. For the stator and rotor areas, the magnetization curve is very essential.

The FEMM has its materials library that contains the magnetic properties for quiet enough number of materials. For SRM, it is needed to define the magnetic properties for three materials. The air-gap can be defined as air, and the coils can be defined as copper (for example, 18 AWG). The type of steel core differs from machine to another; it should be defined carefully according to its steel type. Generally M-19, M-27, M-36, M-43, M-47, and M-50 are mostly used in rotary electric machines.

Before defining the material properties, it should be first added to the FEMM file using function (`mi_getmaterial`) as follows:

```
%% Add materials
mi_getmaterial('Air');
mi_getmaterial('18 AWG'); % copper
mi_getmaterial('Cold rolled low carbon strip steel'); % Steel core
```

The added materials are fully defined within the FEMM. So there is no need for more definitions. If it is necessary to change the material definitions, one can use function (`mi_modifymaterial`). If the material does not exist in FEMM materials library, one can use function (`mi_addmaterial`), but it is needed to define the material carefully.

Once all the materials are added and fully defined as desired, they should be included in the drawn geometry as shown in **Figure 6**. The shaft is defined as air, the rotor and stator iron are defined as cold rolled low carbon strip steel, the air-gap is defined as air, and the windings are defined as 18-AWG copper.

To achieve that, first you should add block label in each area, it is needed to set the block properties. This can be done by using (`mi_addblocklabel`, `mi_setblockprop`) functions.

4.2.2.2 Definition of current circuits

Now, it is time to define the current circuit for copper windings. In our case for 8/6 SRM, there are four independent phases (A, B, C, D). Each phase consists of two coils located at two opposite poles. The direction of current in motor windings must make magnetic field direction generated by both phase windings to be coherent. The flux will flow out from one pole to enter its opposite pole. According to the current direction in the coils, one pole is north and the other is south. It should be noted that, the current direction in FEMM is always positive, there is no negative currents, but it can be achieved if the number of turns is set to negative. The two coils on two opposite poles can be connected either in parallel or series.

Figure 7 shows the sign for the turns number for phase A. the pole on right is north and the other on left is south. If the turns are set wrong, for example both poles are north or both are south, the flux will diminish each other and the resultant flux will be almost zero.

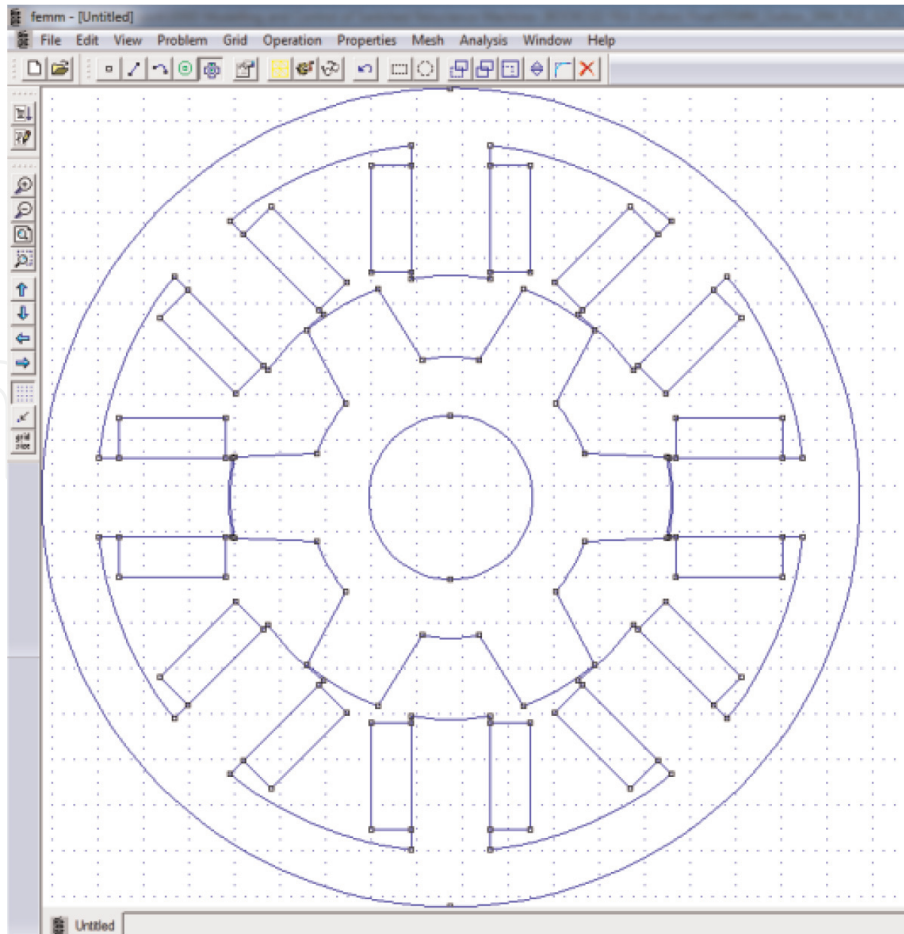


Figure 5.
The final drawn geometry of 8/6 SRM.

To add the circuit properties, the function (`mi_addcircprop`) can be used. Then the properties of the previously defined 18 AWG blocks can be set to include the circuits. A code example is given below:

```
mi_addcircprop(A, i, 1); % add the circuit properties

%% To draw phase A (on the wright and above)
mi_selectlabel(x_a, y_a);
mi_setblockprop('18 AWG', auto_mesh, mesh_size, A, 30, group, -N);
mi_clearselected;

%% To draw phase A (on the wright and below)
mi_selectlabel(x_a, -y_a);
mi_setblockprop('18 AWG', auto_mesh, mesh_size, A, 30, group, N);
mi_clearselected;

%% To draw phase A (on the left and above)
mi_selectlabel(-x_a, y_a);
mi_setblockprop('18 AWG', auto_mesh, mesh_size, A, 30, group, -N);
mi_clearselected;

%% To draw phase A (on the wright and below)
mi_selectlabel(-x_a, -y_a);
mi_setblockprop('18 AWG', auto_mesh, mesh_size, A, 30, group, N);
mi_clearselected;
```

Each phase is defined by 4 copper blocks as shown in **Figure 7**. The four copper blocks should be included in the circuit with proper connection as described by the given code above. The (x, y) coordinates for each block are defined by (x_a, y_a). If

FEMM is set to automatically choose mesh size, then $\text{auto_mesh} = 1$. Otherwise $\text{auto_mesh} = 0$ and mesh_size should be chosen as desired. N is the number of turns per pole.

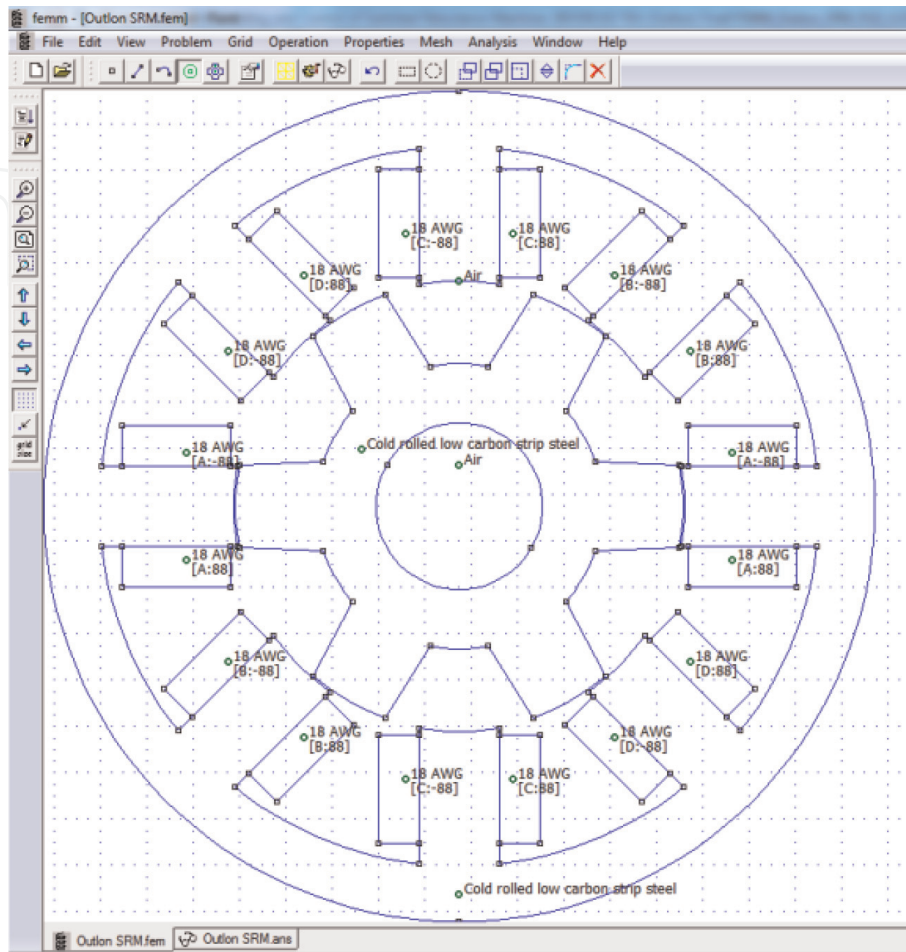


Figure 6.
The final drawn geometry with materials definitions.

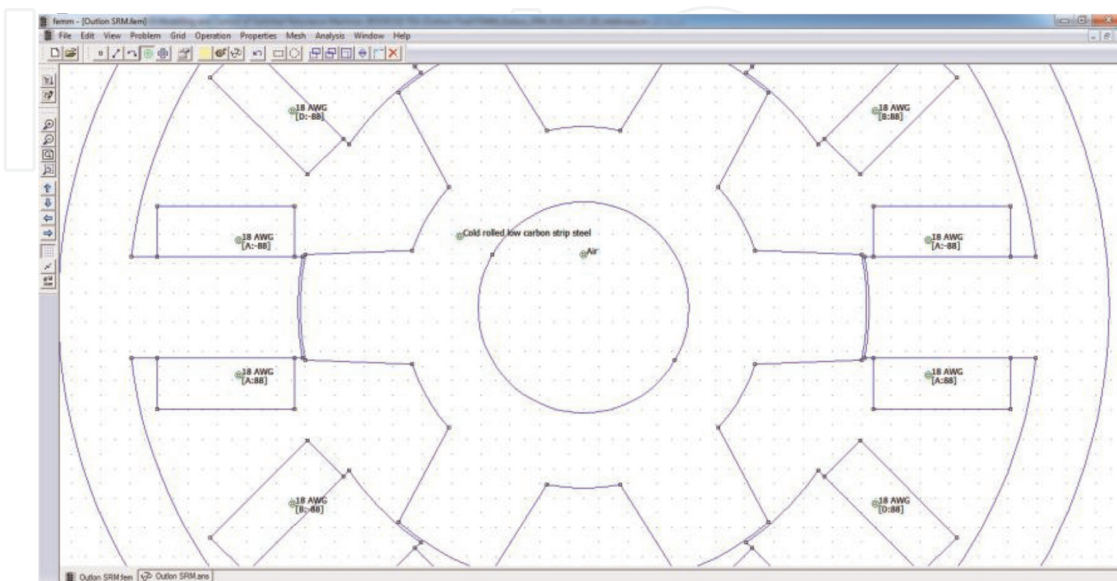


Figure 7.
Setting the number of turns for one phase.

4.2.2.3 Definition of boundary conditions

It is needed to specify the area where the magnetic field is confined within the motor. A negligible flux leakage can be observed outside the stator, so the yoke circumference can be defined as a zero potential vector ($A = 0$). Dirichlet boundary conditions are the best choice for such problems.

```

%% Set boundary conditions
mi_addboundprop('A=0', 0, 0, 0, 0, 0, 0, 0, 0, 0);
mi_selectarcsegment(Doy/2,0);
mi_setarcsegmentprop(2.5,'A=0', 0, 2);
mi_clearselected;

mi_selectarcsegment(-Doy/2,0);
mi_setarcsegmentprop(2.5,'A=0', 0, 2);
mi_clearselected;
    
```

4.3 Results of FE analysis

In 2D FEA, the solution accuracy depends on field nature and mesh size. The mesh size for any component of the entire model can be controlled by FEMM. **Figure 8** shows two different mesh sizes at the unaligned rotor position ($\theta = 0^\circ$) regarding phase A.

To obtain the solution, the value of phase current must be specified. This is done by applying a current driven source for a certain phase using `mi_setcurrent('A',i)` Octave function, and i is the value of the desired current. The phase current values used to obtain the model are between 0A and 30A with 1A increment. The rotor angles are changed from unaligned rotor position ($\theta = 0^\circ$) to the aligned rotor position ($\theta = 30^\circ$) with step of 0.5° . These current and angle resolutions are small enough to achieve high accuracy model for the studied 8/6 SRM. The FEMM analysis is achieved using `mi_analyze`; `mi_loadsolution` Octave functions.

Once a solution is obtained, the magnetic potential vector distribution is known, and hence the magnetic flux in each phase can be calculated. The flux density

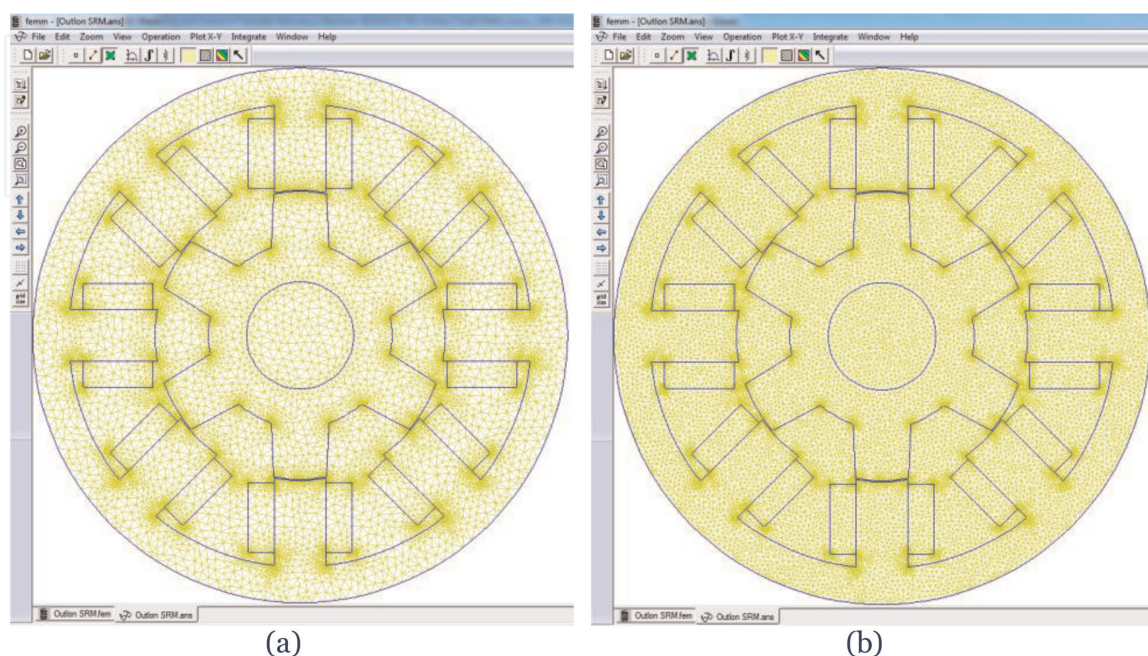


Figure 8.
The mesh size for SRM with (a) 23,473 nodes and (b) 28,703 nodes.

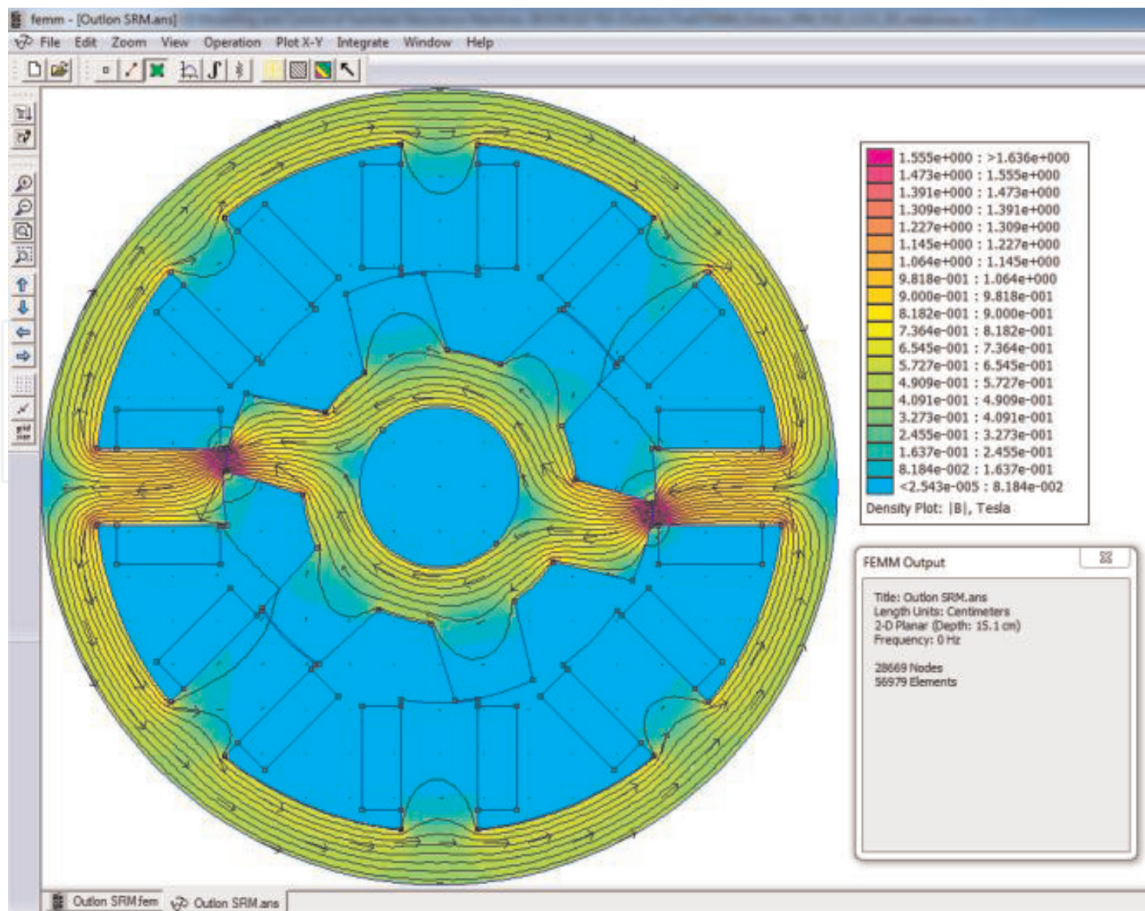


Figure 9.
 The flux density distribution at 15° with excitation current 10 A.

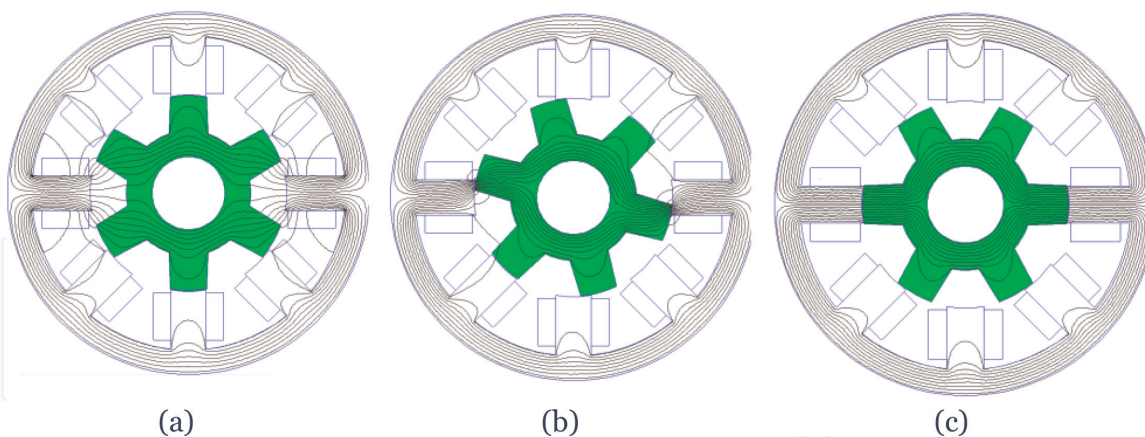
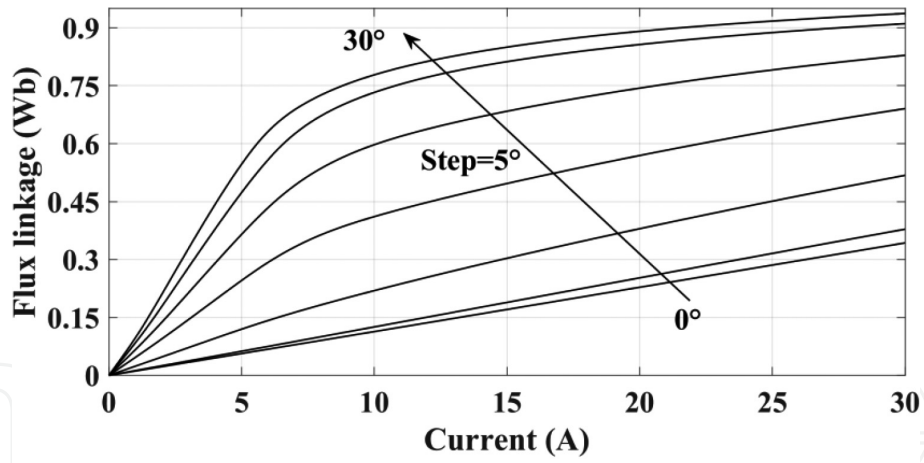


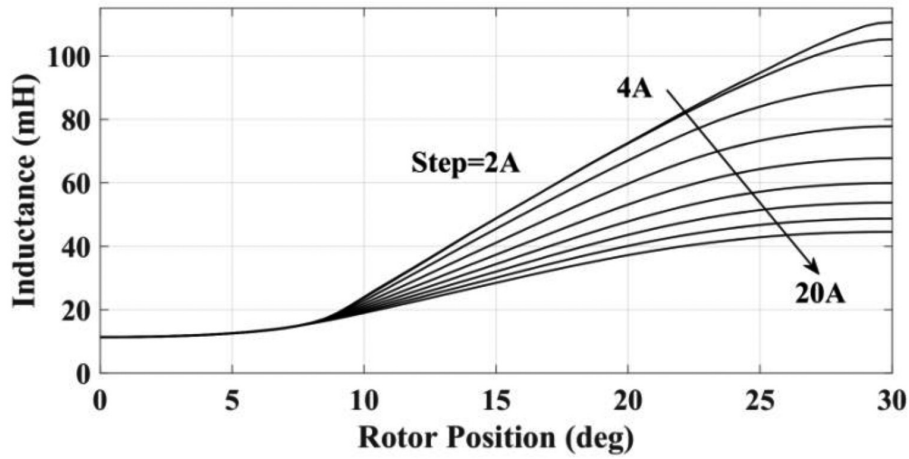
Figure 10.
 The flux lines at different rotor positions with 10 A: (a) 0° , (b) 15° , (c) 30° .

distribution at $\theta = 15^\circ$ with an excitation current of 10(A) is shown in **Figure 9**. The flux lines at different rotor positions are shown in **Figure 10**.

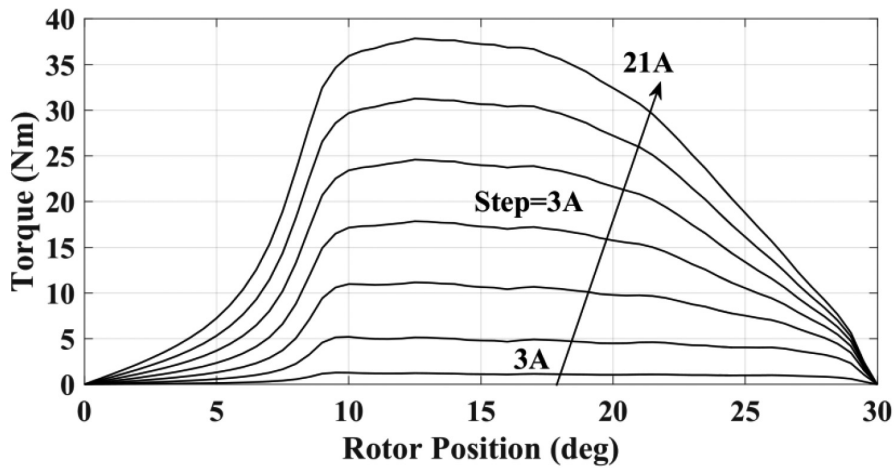
The Magnetic flux linkage in phase A as a function of rotor position and excitation current as obtained by the finite element model is shown in **Figure 11(a)**. Once the flux linkage is obtained, the inductance profile can be deduced according to Eq. (13) as shown in **Figure 11(b)**. The air-gap torque produced on phase A as a function of the rotor position and excitation current as calculated by the finite-element model is shown in **Figure 11(c)**. The doubly salient structure makes the flux, inductance and torque highly nonlinear functions of current magnitude (i) and rotor position (θ).



(a)



(b)



(c)

Figure 11.

The FEM-calculated characteristics for the studied 8/6 SRM. (a) Flux linkage for 8/6 SRM. (b) Inductance for 8/6 SRM. (c) Torque for 8/6 SRM.

$$L(i, \theta) = \lambda(i, \theta) / di \quad (13)$$

5. Experimental measurement methods

Generally, the experimental measurements can be categorized into direct and indirect methods [21, 24]. The direct methods utilize magnetic sensors to directly measure pole flux [24], or they may measure the pole flux directly after proper processing of induced voltage over search-coil that is mounted on stator pole [14].

The direct methods are rarely used because of the leakage flux that affects the accuracy [24]. On the other hand, indirect methods uses phase voltage and current to estimate flux [12]. They can provide simple structure, low cost, and better accuracy [24]. Hence, they are adopted in this work.

5.1 Measuring method and platform

The phase voltage (V) and current (i) are used to measure phase flux linkage indirectly. At a desired rotor position (θ), a pulsed dc voltage is applied to one phase winding, and the phase voltage and current are measured and recorded. The flux-linkage (λ) is calculated according to Eq. (10) or its discrete form in Eq. (11) [14].

$$\lambda(i, \theta) = \int (V - R \cdot i) \cdot dt + \lambda(0) \quad (14)$$

$$\lambda(n) = \sum_{k=1}^n [V(k) - R \cdot i(k)] \cdot T_s + \lambda(0) \quad (15)$$

where R , n , T_s are the phase resistance, adopted number of samples and sampling period, respectively. $\lambda(0)$ is the initial pole flux. It equals to zero because SRM has no magnets.

The same principle is used for torque measurement, but the phase current and torque signals are measured and recorded directly while rotor is locked at a specific position. The measurement procedure of flux/torque should be repeated several times owing to the desired angle resolution to generate the complete flux/torque data. **Figure 12** shows the schematic diagram of measurement platform.

5.2 Measurement results

As SRM has an identical geometrical structure, only one phase can be used for measurement, and only half electric period of 30° mechanical degrees are adopted for measurement. The remaining part of characteristics can be estimated by proper

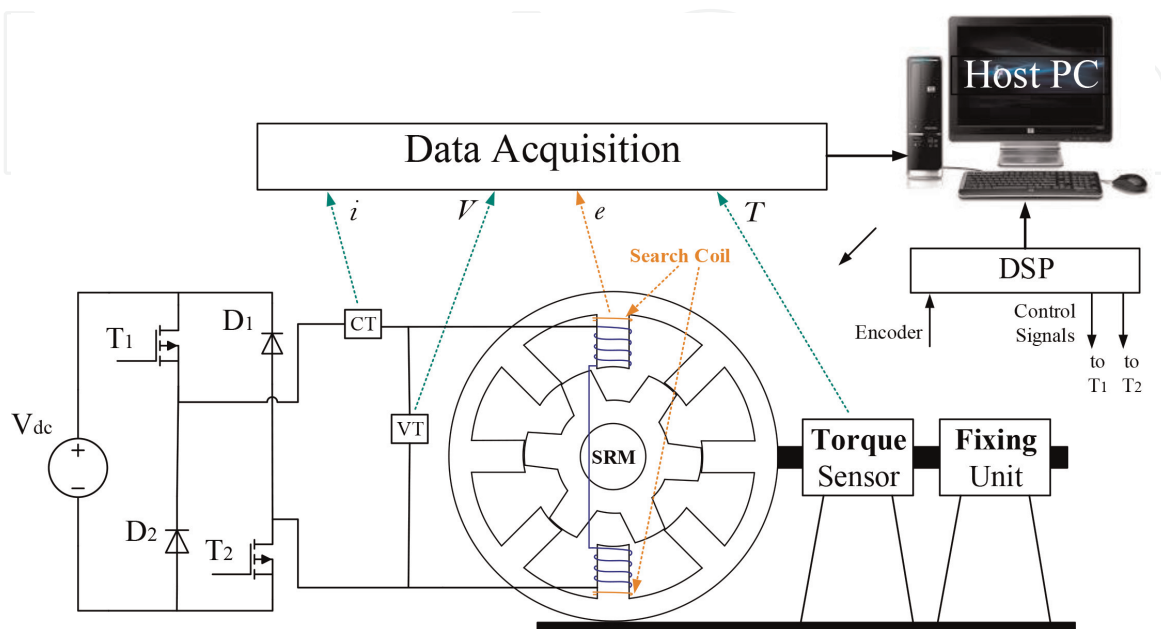
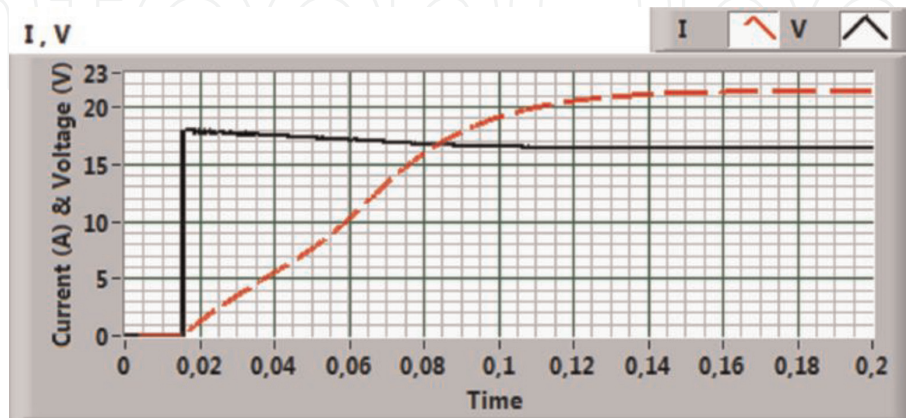


Figure 12.
 The wiring diagram for the measurement platform.

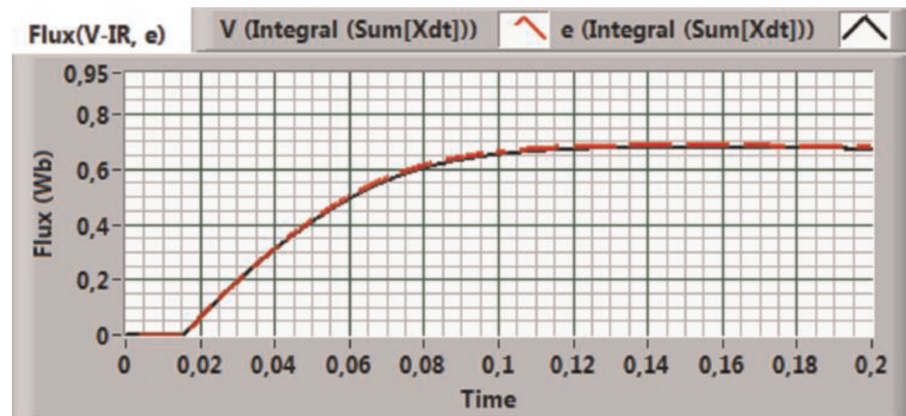
mirroring. The measurement process starts at the unaligned position ($\theta = 0^\circ$) and ends at the aligned position ($\theta = 30^\circ$).

5.2.1 The measured results of flux-linkage

The tested 8/6 SRM is equipped with a search coil on stator poles. The search coil is used for verification purposes. The integration of voltage (e) induced on search coil gives directly the phase flux linkage. The measured phase voltage and current



(a)



(b)

Figure 13.
The measured waveforms at 17° for (a) voltage and current, (b) flux.

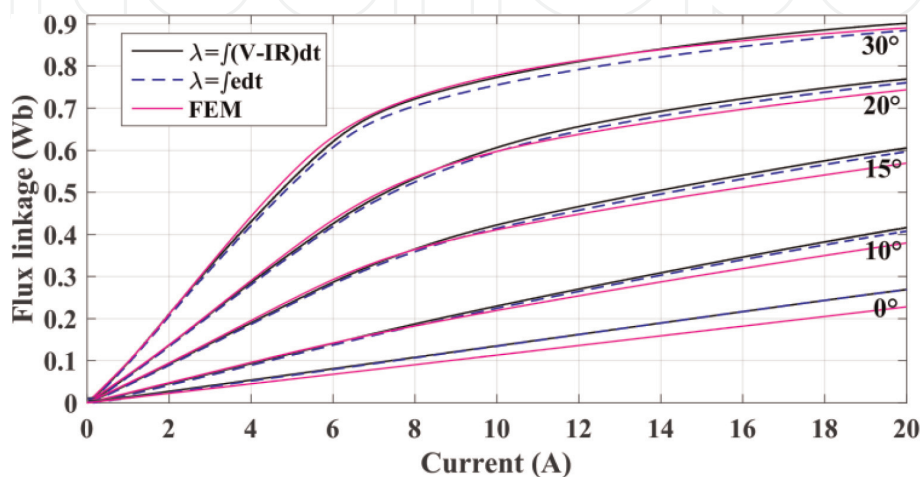


Figure 14.
The measured and FEM flux curves.

are given in **Figure 13(a)**. Their corresponding measured flux linkage is illustrated in **Figure 13(b)**. The adopted current for measurements is 20A with positioning step of 1° . **Figure 14** shows the obtained flux curve at five different rotor positions. It compares between the direct, indirect, and FEA methods. A very good agreement can be seen.

5.2.2 The measured results of static torque

The electromagnetic torque of the SRM is measured directly using a DRBK torque sensor. The DRBK has a limited sampling frequency of 1 kHz. This may affect the measurement accuracy. Better accuracy can be achieved if it is possible to measure reasonable number of samples. This can be achieved by increasing the measurement time. This time is the rising time of phase current. Adding an external inductance in series with phase winding can extend measurement time. The added inductance can increase time constant. Hence, current increase becomes slower allowing recording more torque samples. **Figure 15** shows the measured torque signal along with phase current at position of 16.5° . The measured torque curves are shown in **Figure 16**. **Figure 17** shows a comparison between measured and FEM-calculated torque characteristics, a very good agreement is observed.

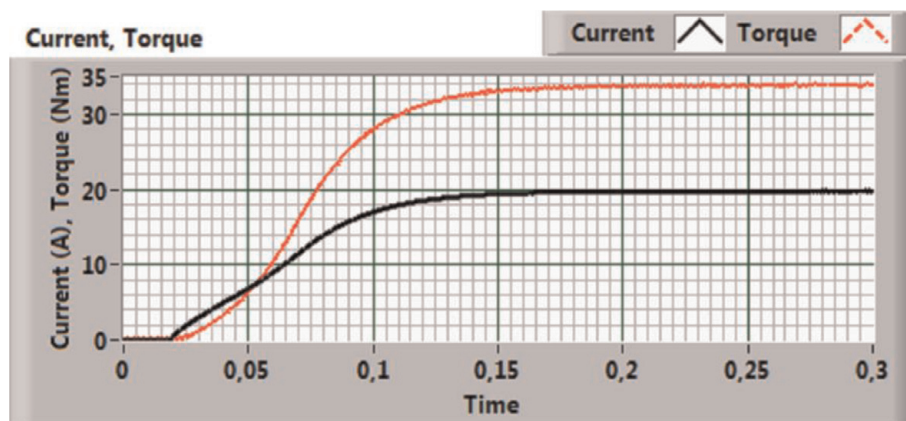


Figure 15.
The measured current and torque waveforms at 16.5° .

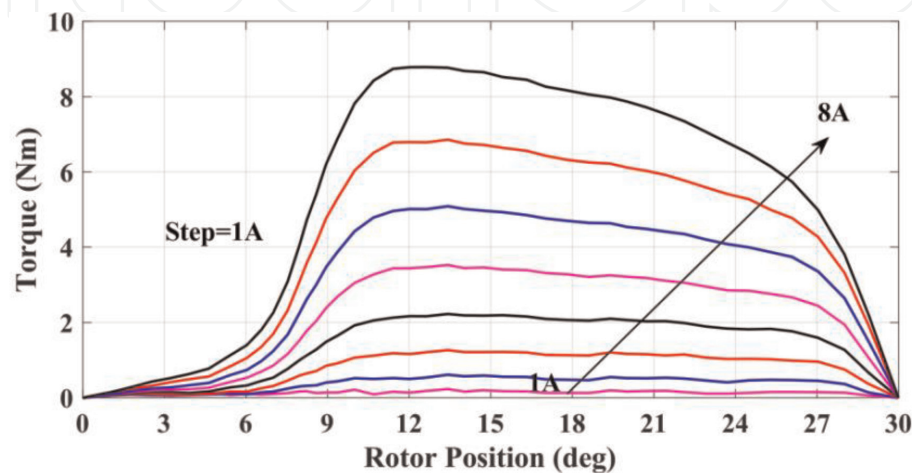


Figure 16.
The measured torque curves.

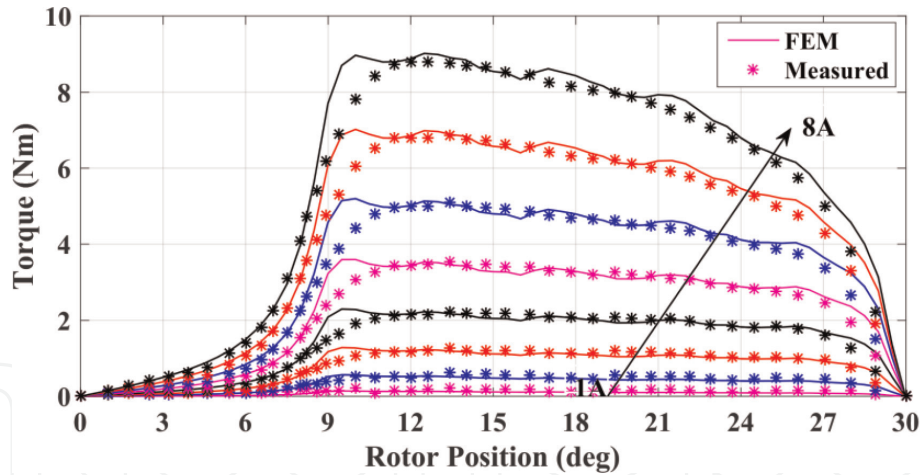


Figure 17.
The measured and FEM torque curves from 1A to 8A.

5.3 Error analysis and minimization

There are several introduced errors during measurement process such as signal errors, parameter errors, and calculation errors. These errors need to be well post-processed to reduce them.

The signal errors include sensor-offsets and nonlinearities, electronics noises, and the quantization errors. Therefore, the voltage and current transducers need precise inspection to compensate signal error. The quantization errors can be reduced through differential connection of DAQ. In this connection, the analog to digital converter (ADC) of DAQ can achieve higher resolution that can ensure minimized quantization errors.

The parameter errors include rotor position and phase resistance. These errors happen as measured values differ from their actual values. The variation of phase resistance can be reduced by two methods. A dc measurement of phase resistance can be done several times while the average value is reported as the real one. Besides, the temperature effect on coil resistance can be minimized by using very low frequency (< 1 Hz) voltage pulses [7, 10]. The rotor position error comes from the encoder itself as the SRM is locked in a certain position. Therefore, in order to reduce rotor position error, a small angular step encoder is advised.

The calculation errors occur mainly because of the numeric integration. These errors depend on integration method and the sampling frequency. If a too low sampling frequency is used, the voltage and current waveforms will be distorted. Hence, the truncation errors of the numerical calculations will increase. On the contrary, if a too high sampling frequency is adopted, the rounding error will increase because of the huge number of computations.

6. Model development using MATLAB/Simulink

The switched reluctance drive system simulation is more complex than DC and AC drives. The dynamic simulation is carried out based on its mathematical model that is given through Eq. (16) to Eq. (24). These equations are solved simultaneously using MATLAB/Simulink.

6.1 Mathematical model of SRM

Due to the double salient structure, the flux linkage $\lambda(i, \theta)$, inductance $L(i, \theta)$, and torque $T(i, \theta)$ are functions of both current magnitude (i) and rotor position (θ).

In $\frac{3}{4}$ phases SRMs, almost two phases conduct simultaneously. The incoming and outgoing phases are denoted as k^{th} and $(k-1)^{th}$ phases respectively. The phase voltage equations can be derived as follows [24, 34]:

$$v_k = Ri_k + \frac{d\lambda_k}{dt}, \quad v_{k-1} = Ri_{k-1} + \frac{d\lambda_{k-1}}{dt} \quad (16)$$

where v_k and v_{k-1} are the voltage for incoming and outgoing phases respectively. i_k and i_{k-1} are the current for incoming and outgoing phases respectively. When mutual flux is considered, flux linkage for incoming (λ_k) and outgoing (λ_{k-1}) phases can be expressed as:

$$\lambda_k = \lambda_{k,k} + \lambda_{k,k-1}, \quad \lambda_{k-1} = \lambda_{k-1,k-1} + \lambda_{k-1,k} \quad (17)$$

where $\lambda_{k,k}$ and $\lambda_{k-1,k-1}$ are the self-flux linkages of k^{th} and $(k-1)^{th}$ phases respectively. $\lambda_{k,k-1}$ and $\lambda_{k-1,k}$ are the mutual flux linkages.

The flux linkage can be represented as Eq. (18) in terms of self and mutual inductances.

$$\begin{bmatrix} \lambda_k \\ \lambda_{k-1} \end{bmatrix} = \begin{bmatrix} L_{k,k} & M_{k,k-1} \\ M_{k-1,k} & L_{k-1,k-1} \end{bmatrix} \begin{bmatrix} i_k \\ i_{k-1} \end{bmatrix} \quad (18)$$

where $L_{k,k}$ and $L_{k-1,k-1}$ are the self-inductances of the k^{th} and $(k-1)^{th}$ phases respectively. $M_{k,k-1}$ and $M_{k-1,k}$ are the mutual inductances.

Considering magnetic saturation, the phase voltage equations are derived as:

$$\begin{aligned} \begin{bmatrix} v_k \\ v_{k-1} \end{bmatrix} &= R \begin{bmatrix} i_k \\ i_{k-1} \end{bmatrix} + \begin{bmatrix} L_{inc_k} & M_{inc_k,k-1} \\ M_{inc_k-1,k} & L_{inc_k-1} \end{bmatrix} \begin{bmatrix} \frac{di_k}{dt} \\ \frac{di_{k-1}}{dt} \end{bmatrix} \\ &+ \omega_m \begin{bmatrix} \frac{\partial L_{k,k}}{\partial \theta} & \frac{\partial M_{k,k-1}}{\partial \theta} \\ \frac{\partial M_{k-1,k}}{\partial \theta} & \frac{\partial L_{k-1,k-1}}{\partial \theta} \end{bmatrix} \begin{bmatrix} i_k \\ i_{k-1} \end{bmatrix} \end{aligned} \quad (19)$$

where ω_m is angular speed of SRM. L_{inc_k} and L_{inc_k-1} are the incremental inductances of the k^{th} and $(k-1)^{th}$ phases respectively. $M_{inc_k,k-1}$ and $M_{inc_k-1,k}$ are the incremental mutual inductances. Incremental inductance and incremental mutual-inductance are given in Eq. (20) and Eq. (21). In linear magnetic region, the incremental inductance is equal to the self-inductance.

$$L_{inc_k} = L_{k,k} + i_k \frac{\partial L_{k,k}}{\partial i_k}, \quad L_{inc_k-1} = L_{k-1,k-1} + i_{k-1} \frac{\partial L_{k-1,k-1}}{\partial i_{k-1}} \quad (20)$$

$$M_{inc_k,k-1} = M_{k,k-1} + i_{k-1} \frac{\partial M_{k,k-1}}{\partial i_{k-1}}, \quad M_{inc_k-1,k} = M_{k-1,k} + i_k \frac{\partial M_{k-1,k}}{\partial i_k} \quad (21)$$

Electromagnetic torque of k^{th} phase can be derived as:

$$T_{e(k)} = \frac{1}{2} \frac{\partial L_{k,k}}{\partial \theta} i_k^2 \quad (22)$$

where $T_{e(k)}$ is the torque produced by k^{th} phase. For SRM with m-phases, the total electromagnetic torque T_e can be represented as:

$$T_e = \sum_{k=1}^m T_{e(k)} \quad (23)$$

The equation for mechanical dynamics is expressed as:

$$T_e - T_L = B\omega_m + J \frac{d\omega_m}{dt} \quad (24)$$

where T_L is the load torque, B is the friction constant, J is the machine inertia.

6.2 Simulation of SRM drive

A simulation model for the experimentally tested 8/6 SRM is achieved using MATLAB Simulink environment. The model can use the data obtained from measurements or from FEA. As discussed earlier in Section 5, both are in a very good agreement, but the measured data have better accuracy. Therefore, the model uses the data obtained from measurements. Using these data, the unwanted approximations introduced by the analytic models are eliminated, the precision of the results is increased and the perspective on the machine is more accurate. To avoid the inaccuracies inherent to the analytical model, the characteristics of current versus rotor position and flux and of torque versus rotor position and current are stored in lookup tables and are introduced in the model of the SRM. In this manner an accurate model of the machine is obtained, capable of providing an objective perspective on the behavior of the SRM under different operating conditions. The model can be further used in the optimization of control and/or design. Although these models are very close to the real behavior of the machine, the mutual coupling between phases, reported by previous work as having a small influence on the machine's operation, is not taken into account [14, 21].

Modeling and simulation of one phase of SRM is shown in **Figure 18**. The inputs are the rotor position (θ) and the phase voltage (V). The outputs are phase current (i) and phase torque (T). The model utilizes the measurement data of flux and torque after proper rearrangement in form of lookup tables [20, 21]. The torque data can be rearranged easily as the torque is measured as a function of current and position $T(i, \theta)$. The hard task appears with the flux data $\lambda(i, \theta)$, as the model calculates current as a function of flux and position $i(\lambda, \theta)$. Hence, the measured flux data $\lambda(i, \theta)$ should be processed and rearranged to produce required current data $i(\lambda, \theta)$. This can be achieved by interpolation and extrapolation of flux data against current for different rotor positions. Due to the enormous measured

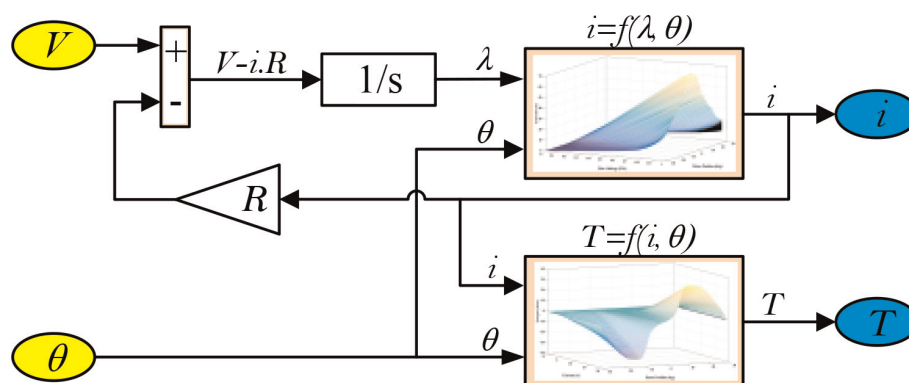


Figure 18.
Simulation of one phase of SRM.

samples of flux, the interpolation and extrapolation of current $i(\lambda, \theta)$ can ensure a sufficient accuracy.

The SRM cannot run directly from an AC or DC source; it requires continuous commutation from one phase to another. So, the motor itself and its converter are considered as one unit. For system simulation, the converter and the position sensing unit need also to be modeled. The most common converter for SRM is the asymmetric bridge converter as shown in **Figure 12** for one phase of SRM. The position sensing unit feeds the controller with the correct position for each phase. According to the phase position, the controller determines the firing angles for this phase. The control defines the switching state for each phase according to the switch-on (θ_{on}) and switch-off (θ_{off}) angles. The voltage $+V$ is applied when ($\theta_{on} = <\theta < \theta_{off}$) and the voltage is $-V$ when ($\theta > \theta_{off}$). The phase currents of the motor can

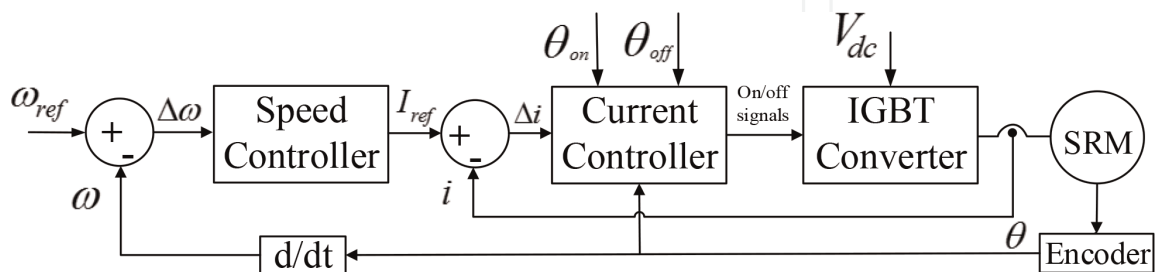


Figure 19.
 Block diagram of SRM control system.

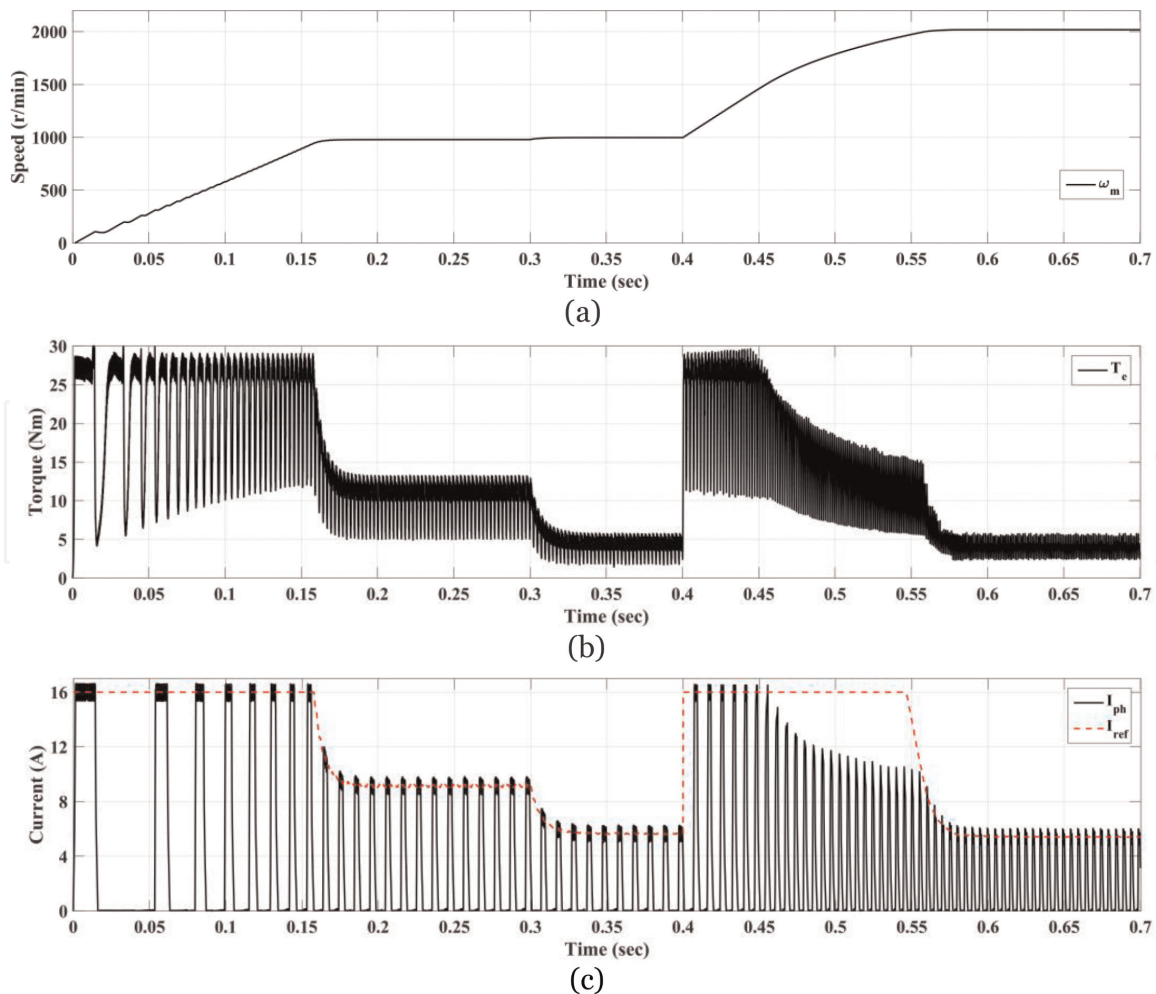


Figure 20.
 Simulation results under transient conditions: (a) motor speed; (b) the total electromagnetic torque; and (c) the reference current and one phase current.

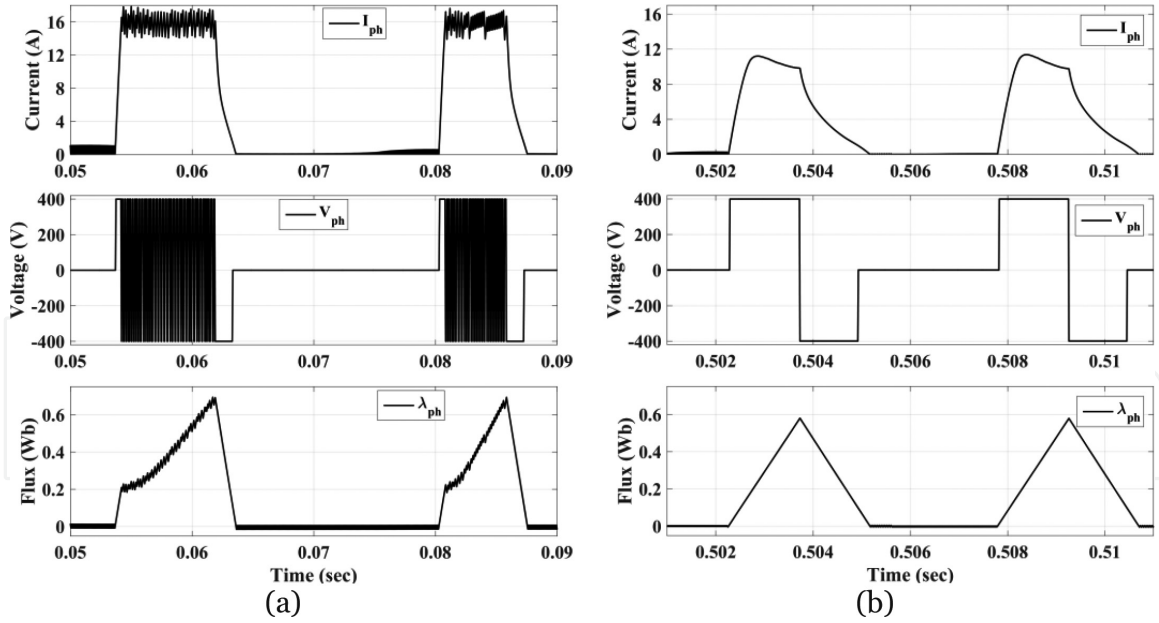


Figure 21. Simulation results under (a) low speed and (b) high speed.

be limited using chopping process. The block diagram of SRM control system is shown in **Figure 19**. It has an outer loop speed controller that outputs the reference current signal (I_{ref}) according to speed error signal ($\Delta\omega$). An inner loop current controller is needed to regulate motor phase current (i) to track its reference current. A feedback of rotor position is essential for motor operation.

6.2.1 Simulation results

The SRM operates in two modes according to the motor speed. At low speeds the back-emf is very small compared to the applied voltage, the current increases rapidly after the instant of switching-on. The rapid increase of the phase current must be limited to an allowable value by Hysteresis Current Control (HCC). On the other hand, at high speeds the back-emf is considerable and the current is lower than the permissible value. In this case, the voltage is a single pulse.

Figure 20 shows the simulation results under transient conditions. The motor speed changes from 1000 r/min to 2000 r/min at 0.4 sec. The load torque changes from 10 Nm to 6 Nm at time 0.3 sec. The speed response is shown in **Figure 20(a)**. The total torque is given in **Figure 20(b)**, as noted it has a highly noticeable ripple that is the major drawback for SRMs. **Figure 20(c)** shows the performance of current controller as it regulates phase current to track its reference current.

The current profile under low and high speed is shown in **Figure 21**. For low speed, the current is regulated using HCC, the phase voltage is changed between $+V$ and $-V$ to achieve that control, the shape of phase flux is a little bit away to form a triangular shape as shown in **Figure 21(a)**. For high speeds, the phase voltage becomes a single pulse, the current limitation is no longer in use, the flux becomes a pure triangle as shown in **Figure 21(b)**.

7. Experimental verification

For the detailed experimental verification of the established model, a series of results are obtained. A comparison between the simulated and experimentally

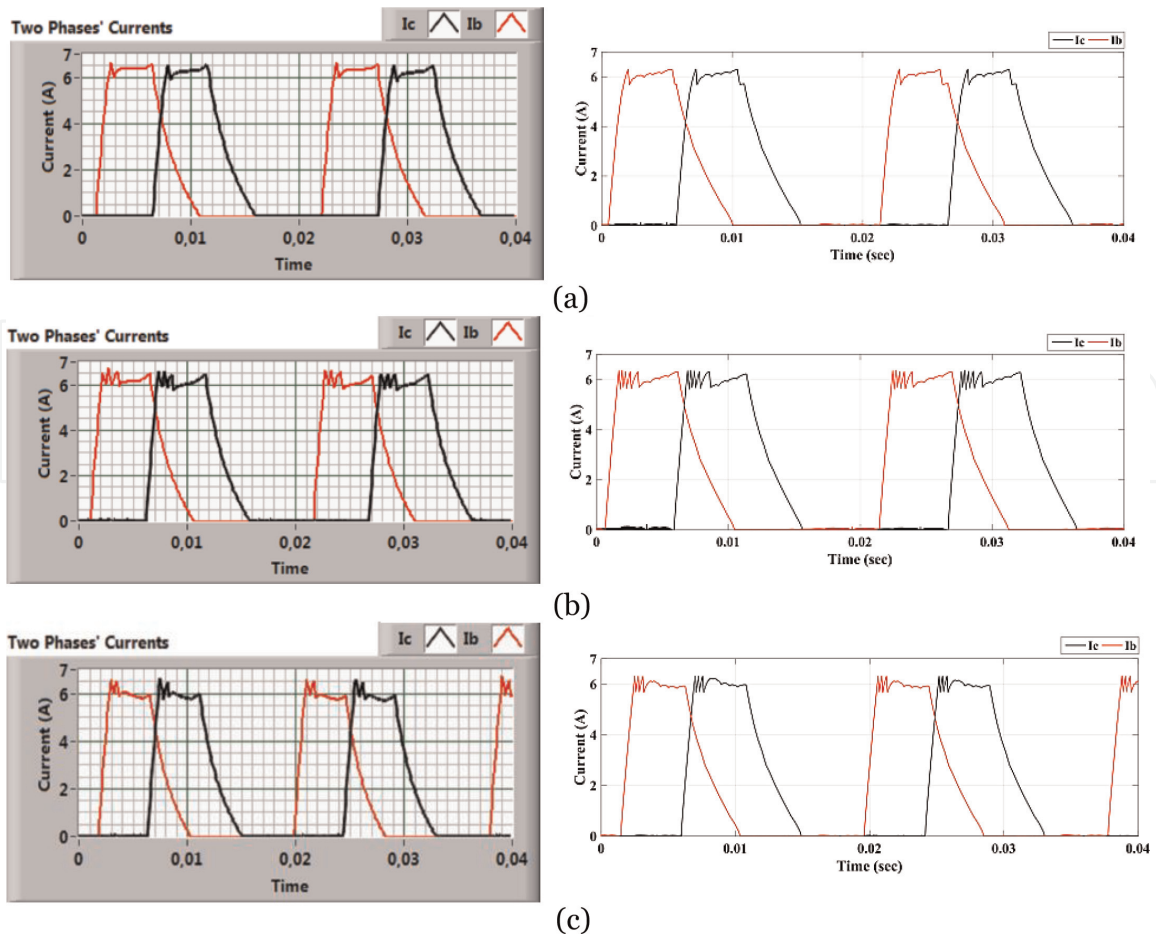


Figure 22. Comparison between the measured and simulated current waveforms: (a) at 480 r/min, $\theta_{on} = 5^\circ$, $\theta_{off} = 20^\circ$; (b) at 481 r/min, $\theta_{on} = 3^\circ$, $\theta_{off} = 19^\circ$; and (c) at 551 r/min, $\theta_{on} = 3^\circ$, $\theta_{off} = 19^\circ$.

obtained current waveforms is achieved for different operating as given in **Figure 22**. As seen a very good agreement is achieved that reflects the modeling accuracy.

8. Conclusions

This chapter explains the modeling and simulation methods for SRMs. It discusses the analytical and intelligent methods for SRM modeling. Besides, it determines the static performance of an 8/6 switched reluctance machine as obtained from the two dimensional finite-element method analysis using FEMM and compares the results with experimental obtained ones. A very good agreement is observed. Then it gives the simulation of the SRM drive system in MATLAB/Simulink environment.

IntechOpen

Author details


Mahmoud Hamouda^{1,2*} and László Számel¹

1 Department of Electric Power Engineering, Budapest University of Technology and Economics, Budapest, Hungary

2 Electrical Engineering Department, Mansoura University, Mansoura, Egypt

*Address all correspondence to: m_hamouda26@mans.edu.eg

IntechOpen

© 2020 The Author(s). Licensee IntechOpen. Distributed under the terms of the Creative Commons Attribution - NonCommercial 4.0 License (<https://creativecommons.org/licenses/by-nc/4.0/>), which permits use, distribution and reproduction for non-commercial purposes, provided the original is properly cited. 

References

- [1] Lin D, Zhou P, Stanton S, Cendes ZJ. An analytical circuit model of switched reluctance motors. *IEEE Transactions on Magnetics*. 2009; **45**(12):5368-5375
- [2] Song S, Zhang M, Ge L. A new decoupled analytical modeling method for switched reluctance machine. *IEEE Transactions on Magnetics*. 2015; **51**(3). Article Number: 8100504
- [3] Hamouda M, Számel L. Optimum control parameters of switched reluctance motor for torque production improvement over the entire speed range. *Acta Polytechnica Hungarica*. 2019; **16**(3):79-99
- [4] Uddin W, Sozer Y. Analytical modeling of mutually coupled switched reluctance machines under saturation based on design geometry. *IEEE Transactions on Industry Applications*. 2017; **53**(5):4431-4440
- [5] Chen H, Jiang D, Yang J, Shi L. A New analytical model for switched reluctance motors. *IEEE Transactions on Magnetics*. 2009; **45**(8)
- [6] Yoopakdee C, Fuengwarodsakul NH. Analytic model of switched reluctance machine using combined Fourier-polynomial approximation technique. In: 2018 XIII International Conference on Electrical Machines (ICEM). Alexandroupoli, Greece; 2018
- [7] Torrey DA, Niu XM, Unkauf EJ. Analytical modelling of variable-reluctance machine magnetisation characteristics. *IEE Proceedings - Electric Power Applications*. 1995; **142**(1):14-22
- [8] Sheth NK, Rajagopal KR. Calculation of the flux-linkage characteristics of a switched reluctance motor by flux tube method. *IEEE Transactions on Magnetics*. 2005; **41**(10):4069-4072
- [9] Vujičić V, Vukosavić SN. A simple nonlinear model of the switched reluctance motor. *IEEE Transactions on Energy Conversion*. 2000; **15**(4): 395-400
- [10] Radimov N, Ben-Hail N, Rabinovici R. Simple model of switched-reluctance machine based only on aligned and unaligned position data. *IEEE Transactions on Magnetics*. 2004; **40**(3):1562-1572
- [11] Zhong R, Xu Y, Cao Y, Guo X, Hua W, Xu S, et al. Accurate model of switched reluctance motor based on indirect measurement method and least square support vector machine. *IET Electric Power Applications*. 2016; **10**(9): 916-922
- [12] Song S, Ge L, Ma S, Zhang M, Wang L. Accurate measurement and detailed evaluation of static electromagnetic characteristics of switched reluctance machines. *IEEE Transactions on Instrumentation and Measurement*. 2015; **64**(3):704-714
- [13] Kiyota K, Kakishima T, Sugimoto H, Chiba A. Comparison of the test result and 3D-FEM analysis at the knee point of a 60 kW SRM for a HEV. *IEEE Transactions on Magnetics*. 2013; **49**(5): 2291-2294
- [14] Hamouda M, Számel L. Accurate measurement and verification of static magnetization characteristics for switched reluctance motors. In: *IEEE 19th International Middle East Power System Conference (MEPCON)*, Cairo, Egypt. 2017. pp. 993-998
- [15] Zhang J, Radun AV. A new method to measure the switched reluctance motor's flux. *IEEE Transactions on Industry Applications*. 2006; **42**(5): 1171-1176
- [16] Lachman T, Mohamad TR, Fong CH. Nonlinear modelling of

switched reluctance motors using artificial intelligence techniques. IEE Proceedings - Electric Power Applications. 2004;**151**(1):53-60

[17] Lin Z, Reay DS, Williams BW, He X. Online modeling for switched reluctance motors using B-spline neural networks. IEEE Transactions on Industrial Electronics. 2007;**54**(6): 3317-3322

[18] Ding W, Liang D. Modeling of a 6/4 switched reluctance motor using adaptive neural fuzzy inference system. IEEE Transactions on Magnetics. 2008; **44**(7):1796-1804

[19] Gouda E, Hamouda M, Amin ARA. Artificial intelligence based torque ripple minimization of switched reluctance motor drives. In: 2016 Eighteenth International Middle East Power Systems Conference (MEPCON), Cairo, Egypt. 2016. pp. 943-948

[20] Husain I, Hossain SA. Modeling, simulation, and control of switched reluctance motor drives. IEEE Transactions on Industrial Electronics. 2005;**52**(6):1625-1634

[21] Hamouda M, Számel L. Accurate magnetic characterization based model development for switched reluctance machine. Periodica Polytechnica Electrical Engineering and Computer Science. 2019;**63**(3):202-212

[22] Spong MI, Marino R, Peresada SM, Tayler DG. Feedback linearizing control of switched reluctance motors. IEEE Transactions on Automatic Control. 1987;**AC-32**(5):371-379

[23] Torrey DA, Lang JH. Modeling a nonlinear variable-reluctance motor drive. Proceedings of the Institution of Electrical Engineers. IEEE Proceedings B - Electric Power Applications. Sept. 1990;**137**(5):314-326

[24] Nasirian V, Kaboli S, Davoudi A, Moayedi S. High-fidelity magnetic

characterization and analytical model development for switched reluctance machines. IEEE Transactions on Magnetics. 2013;**49**(4):1505-1515

[25] Xue XD, Cheng KWE, Ho SL, Kwok KF. Trigonometry based numerical method to compute nonlinear magnetic characteristics in switched reluctance motors. IEEE Transactions on Magnetics. 2007;**43**(4):1845-1848

[26] Khalil A, Husain I. A Fourier series generalized geometry-based analytical model of switched reluctance machines. IEEE Transactions on Industry Applications. 2007;**43**(3):673-684

[27] Song S, Zhang M, Ge L. A new decoupled analytical modeling method for switched reluctance machine. IEEE Transactions on Magnetics. 2015;**51**(3): 1-4

[28] Lu W, Keyhani A, Fardoun A. Neural network based modeling and parameter identification of switched reluctance motors. IEEE Transactions on Energy Conversion. 2003;**18**(2): 284-290

[29] Chen H, Han G, Yan W, Lu S, Chen Z. Modeling of a switched reluctance motor under stator winding fault condition. IEEE Transactions on Applied Superconductivity. 2016;**26**(4)

[30] Cheok AD, Ertugrul N. Use of fuzzy logic for modeling, estimation, and prediction in switched reluctance motor drives. IEEE Transactions on Industrial Electronics. 1999;**46**(6):1207-1224

[31] Lachman T, Mohamad TR, Fong CH. Nonlinear modelling of switching reluctance motors using artificial intelligence techniques. IET Electric Power Applications. 2004; **151**(1):23-60

[32] Hamouda M, Gouda E, Amin ARA. Performance Analysis of Switched Reluctance Machine. Mansoura

University, Mansoura city, Egypt; 2015.
pp. 1-171

[33] Meeker D. Finite Element Method
Magnetics: OctaveFEMM. Version 1.2,
User's Manual; 2010. 59p. Available
From: [http://www.femm.info/Archives/
doc/octavefemm.pdf](http://www.femm.info/Archives/doc/octavefemm.pdf)

[34] Ye J. Advanced Control Methods for
Torque Ripple Reduction and
Performance Improvement in Switched
Reluctance Motor Drives. Hamilton,
Ontario: McMaster University; 2014

IntechOpen